THE JOURNAL OF PHYSICAL CHEMISTRY C

Article

pubs.acs.org/JPCC

Role of the Charge-Transfer State in Reduced Langevin Recombination in Organic Solar Cells: A Theoretical Study

Yiming Liu,[†] Karin Zojer,*[,‡] Benny Lassen,[†] Jakob Kjelstrup-Hansen,[†] Horst-Günter Rubahn,[†] and Morten Madsen*[,†]

[†]NanoSYD, Mads Clausen Institute, University of Southern Denmark, Alsion 2, DK-6400 Sønderborg, Denmark

[‡]Institute of Solid State Physics, Graz University of Technology and NAWI Graz, Petersgasse 16, 8010 Graz, Austria

Supporting Information

ABSTRACT: Reduced Langevin recombination has been observed in organic solar cells (OSCs) for many years, but its origin is still unclear. A recent work by Burke et al. (*Adv. Energy Mater.* **2015**, *5*, 1500123-1) was inspired by this reduced Langevin recombination, and they proposed an equilibrium model of charge-transfer (CT) states that correlates the open-circuit voltage of OSCs with experimentally available device parameters. In this work, we extend Burke et al.'s CT model further and for the first time directly correlate the reduced Langevin recombination with the energetic and dynamic behavior of the CT state. Recombination through CT states leads in a straightforward manner to a decrease in the Langevin reduction factor with increasing temperature, without explicit consideration of the temperature dependence of the mobility. To verify the correlation between the CT states and reduced Langevin recombination, we incorporated this CT model and the reduced Langevin model into drift-diffusion simulations of a bilayer OSC. The simulations not only successfully reproduced realistic current−voltage (J−V) characteristics of the bilayer OSC, but also demonstrate that the two models consistently lead to same value of the apparent Langevin reduction factor.

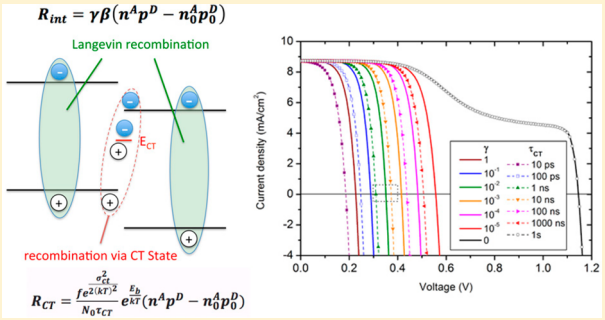

1. INTRODUCTION

High-performance organic solar cells (OSCs) have demonstrated efficient photogeneration of charge carriers with >90% quantum efficiencies,[1] but their power conversion efficiencies are still lower than those of their inorganic counterparts. This can mainly be attributed to their relatively low open-circuit voltages (V_{oc}), compared to the optical bandgap, and their relatively low fill factors (FFs), especially for optically thick devices. The donor/acceptor interface in OSCs plays an important role in the photocurrent generation process as it provides the energy offset needed to dissociate the photogenerated excitons. The recombination at this interface dominates the loss of free charges and, hence, significantly affects V_{oc}.[2] Several experimental techniques have been developed to quantitatively extract recombination rates in organic bulk heterojunction (BHJ) devices.[3−5] For many high-efficiency OSC systems, it has been found that recombination occurs predominantly through bimolecular recombination. The experimentally measured recombination rates in BHJ devices were found to be several orders of magnitude smaller than those predicted by Langevin theory, which is the most commonly used model to describe bimolecular recombination in homogeneous organic materials.

The fundamental origin of such a reduced Langevin recombination rate is still under debate (see, e.g., ref 5). To comprehend the foundation of this debate, it is useful to point out the starting point that is common to all explanation attempts: Onsager's description of bimolecular recombination.[6] It states that recombination involves two stages, each being associated with a rate: The *first rate* describes the likelihood that two oppositely charged particles meet and form a pair of Coulomb-bound charges. This process can be counteracted by a possible dissociation back into independent mobile charges. The *second rate* describes the subsequent recombination of the electron hole pair so that charge-neutral molecules in their ground state are restored. The multitude of suggested explanations stems from different assessments of the extents to which the two rates limit the net recombination. In the case that the first rate is limiting, the original Langevin theory applies.[6] This is certainly valid for most pristine organic materials because of their rather low charge-carrier mobilities. The fact, however, that the straightforward Langevin theory overestimates the recombination rates in BHJ devices indicates that bimolecular recombination at interfaces formed between two organic semiconductors calls for a substantially extended description.

A major line of research aims at clarifying the nature of the first encounter at the organic−organic interface[7−10] and accepts

Received: September 14, 2015
Revised: October 16, 2015
Published: October 26, 2015

DOI: 10.1021/acs.jpcc.5b08936
J. Phys. Chem. C 2015, 119, 26588−26597

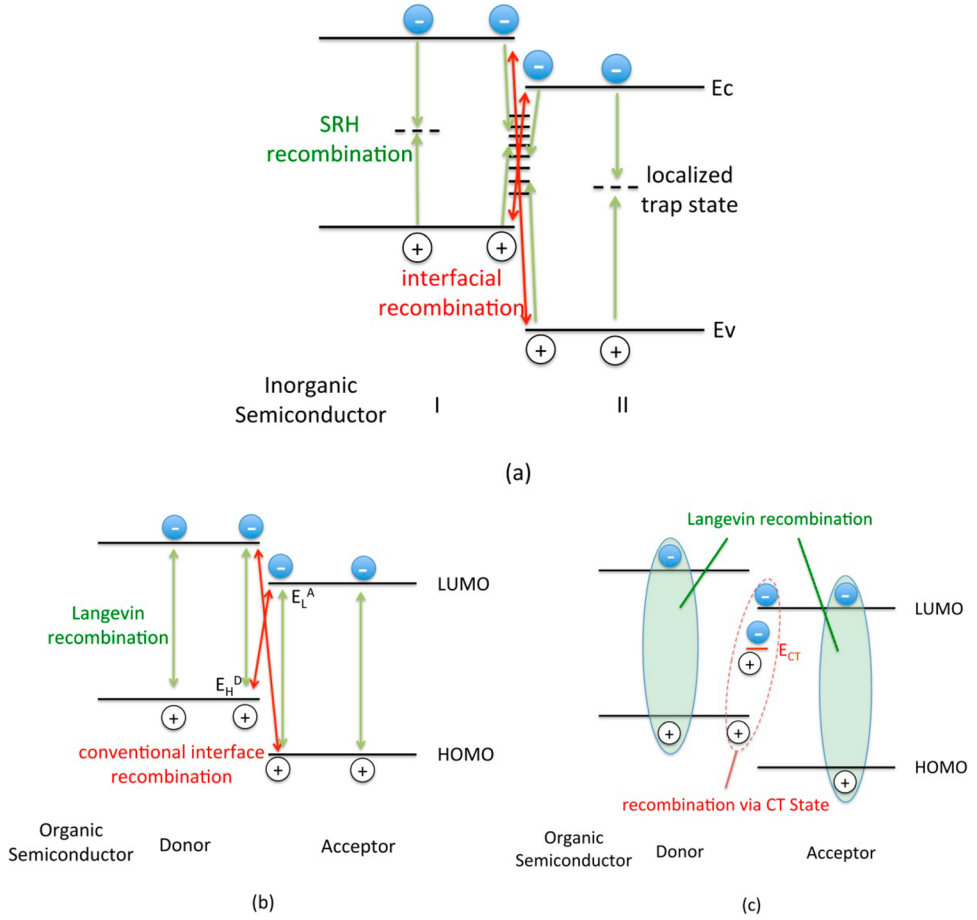

Figure 1. Energy band diagrams of heterointerfaces for (a) inorganic solar cells and (b,c) organic solar cells. (a) Recombination in the bulk is Shockley–Read–Hall (SRH) recombination through localized trap states. E_c and E_v denote the energies of the conduction band and the valence band, respectively, of each material. The recombination at the interface consists of four paths: Two paths are SRH recombination between local carriers, and the other two SRH-like paths are between the electrons and holes from different sides of the interface (marked by red arrows). (b) Bimolecular recombination in the bulk of an OSC is described by Langevin theory (represented by green arrows). At the interface, two additional recombination paths (represented by red arrows, similar to the inorganic case) are illustrated. E_L^A and E_H^D denote the positions at the interface of the LUMO level of the acceptor and the HOMO level of the donor, respectively. The energy difference between E_L^A and E_H^D is the effective band gap, E_{DA}, of the OSC. (c) Schematic illustration of interface recombination through CT states.

that recombination occurs instantaneously after pair formation. That is, one assumes that mobile charges recombine directly. As a consequence, V_{oc} is determined from the difference of the associated transport energy levels, that is, the effective gap, E_{DA}, measuring the offset between the highest occupied molecular orbital (HOMO) of the donor and the lowest unoccupied molecular orbital (LUMO) of the acceptor.[11,12]

Another research direction is dedicated to a thorough assessment of the relative impact of the second rate.[13] This direction is currently gaining momentum because of increasing experimental evidence that the recombination process involves a charge-transfer (CT) state formed at the interface.[14,15] In strong contrast to the encounter-limited model, the open-circuit voltage was found to be determined by the energy, E_{CT}, of this interface state.[2,16,17] Burke et al. recently suggested that reduced Langevin recombination implies the existence of an equilibrium between free carriers and populated CT states.[18] The necessary condition is that the redissociation rate of the populated CT states back to free carriers is several times larger than the recombination rate for the transition of the CT state into a neutral ground state, that is, the CT states dissociate several times before ultimately recombining. Assuming an equilibrium situation, the density of populated CT states can be related in a straightforward manner to E_{CT} and the quasi-Fermi levels of free carriers by a Boltzmann distribution. By deriving the interface recombination rate based on the CT state density for open-circuit conditions, one arrives at a concise equation that quantitatively relates V_{oc} to E_{CT}. This equation successfully explains the observed dependence of V_{oc} on the interfacial energetic disorder, temperature, and dielectric constants.[18]

In this work, we explore the applicability of Burke et al.'s model to other steady-state operating conditions of OSCs, namely, beyond open-circuit conditions, because the underlying quasi-equilibrium should hold under these conditions as well. By utilizing drift-diffusion simulations, we directly determined the participation of the CT state from the splitting between the quasi-Fermi levels of electrons and holes and analyzed its effects at each bias voltage. As this approach allows for the simulation of the full current–voltage characteristics, it can be used to predict the impact of the CT states on device parameters, such as the fill factor and the temperature-dependent open-circuit voltage.

DOI: 10.1021/acs.jpcc.5b08936
J. Phys. Chem. C 2015, 119, 26588–26597

2. INTERFACE RECOMBINATION

Before we analyze the effects of interface recombination on device performance through drift-diffusion modeling, we first review the device physics of interface recombination.

2.1. Inorganic Model. In the field of inorganic solar cells, interface recombination at the heterojunction has been studied extensively.[19−22] Recombination in the bulk of inorganic solar cells is usually dominated by the Shockley−Read−Hall (SRH) process, which characterizes carrier recombination in terms of localized trap states.[23] Recombination through the interface states can be treated by an extension of the SRH formalism, adding two more recombination paths (represented by the red arrows shown in Figure 1a) between electrons and holes of two adjacent semiconductors.[24] The addition of these paths is crucial in the case illustrated in Figure 1a, where the dominant interface recombination pathway involves holes of semiconductor I and electrons of semiconductor II. Scheer systematically analyzed the impact of interface recombination paths on the V_{oc} values of heterojunction devices.[21] Generally, V_{oc} can be expressed as[21]

$$V_{oc} = \frac{E_a}{q} - \frac{AkT}{q}\ln\left[\frac{J_{00}}{J_{sc}\eta(V_{oc})}\right] \tag{1}$$

where E_a is the activation energy of the heterojunction diode, q is the electron charge, A is the ideality factor, k is the Boltzmann constant, T is the temperature, J_{00} is the reference current density,[25] J_{sc} is the short-circuit current, and $\eta(V_{oc})$ is the voltage-dependent collection function. The particular temperature dependence of eq 1 suggests a straightforward experimental way to determine the activation energy E_a. The value of E_a corresponds to the intercept of the linearly extrapolated portion of the V_{oc}−T plot to 0 K. The comparison between E_a and the semiconductor band gaps reveals the dominant recombination path within inorganic cells.[26] For instance, for the interface band alignment shown in Figure 1a, E_a will be equal to the energy gap between E_c(II) and E_v(I) if interface recombination dominates over bulk recombination; otherwise, E_a will be equal to the smaller of the two semiconductor band gaps.

2.2. Organic Model. In organic solar cells, losses in V_{oc} are known to be related to the properties of the donor/acceptor interface. However, also in OSCs, V_{oc} can be cast into an expression similar to eq 1. Thus, V_{oc} ought to exhibit an explicit linear dependence on the temperature. Consequently, E_a can be obtained through an extrapolation approach similar to that in the inorganic case.[16] The remaining debate to be settled is whether E_a corresponds to the effective gap at the donor/acceptor interface, $E_{DA} = E_L^A - E_H^D$, or to the energy of the charge-transfer state, E_{CT} (Figure 1b,c).[12] The case associated with the effective gap is described by a reduced Langevin model, whereas the latter case demands the CT recombination model.

2.2.1. Langevin Model. For the low-mobility materials typically used in OSCs, free charge recombination in the bulk is well described by Langevin theory. The Langevin recombination rate R_L is expressed as[27]

$$R_L = \beta(np - n_i^2) \tag{2}$$

where n and p are the densities of electrons and holes, respectively, and n_i is the intrinsic carrier density. The Langevin recombination prefactor β is given by

$$\beta = \frac{q(\mu_n + \mu_p)}{\varepsilon} \tag{3}$$

where μ_n and μ_p are the carrier mobilities for electrons and holes, respectively, and $\varepsilon = \varepsilon_0\varepsilon_r$ is the permittivity of the material with ε_r being the dielectric constant. Staudigel et al. extended eq 2 to describe the recombination rate at the interface, R_{int}, by introducing, similarly to the inorganic case (Figure 1a), two additional bimolecular recombination pathways[28]

$$R_{int} = \beta_1 n^D p^A + \beta_2 n^A p^D \tag{4}$$

where the superscripts D and A denote the carriers located at the donor and acceptor sides, respectively, of the interface. Each of the two pathways is assumed to be characterized by an individual Langevin recombination prefactor

$$\beta_1 = \frac{q(\mu_n^D + \mu_p^A)}{\bar{\varepsilon}}, \quad \beta_2 = \frac{q(\mu_n^A + \mu_p^D)}{\bar{\varepsilon}} \tag{5}$$

where $\bar{\varepsilon}$ is the average dielectric constant of the two adjacent organic layers. However, this formulation, initially proposed for organic light-emitting diodes, overestimates the recombination rates obtained for interfaces in OSCs.[5] To still allow analysis of the recombination rates in terms of Langevin theory, the Langevin reduction factor γ was introduced.[5,7]

A typical arrangement of transports levels at the OSC interface is presented in Figure 1b. The first recombination term in eq 4 (corresponding to an electron in the donor material recombining with a hole in the acceptor material) is negligible in comparison to the second term. Moreover, it is physically more reasonable to define recombination as a process aiming at re-establishing thermal equilibrium, that is, to subtract the intrinsic thermal generation rate to guarantee that the net recombination is zero at thermal equilibrium. Then, the recombination rate R_{int} for direct bimolecular recombination between electrons and holes at the interface is proportional to the carrier concentrations at the interface, n^A and p^D, in excess of the corresponding equilibrium concentrations n_0^A and p_0^D. To preserve a Langevin-type prefactor in the rate constant, the former must be multiplied by the reduction factor γ. Then, the rate R_{int} takes a final form

$$R_{int} = \gamma\beta_2(n^A p^D - n_0^A p_0^D) \tag{6}$$

The value of γ has been empirically determined to adopt values between 10^{-4} and 10^{-1} in bulk heterojunction OSCs and to decrease with increasing temperature.[7] The evaluation of the temperature dependence of the open-circuit voltage, V_{oc}, due to eq 1 reveals an activation energy, E_a, given by the effective donor/acceptor band gap E_{DA}.[29]

2.2.2. CT Model. In the scenario of interface CT states participating in recombination (Figure 1c), free carriers meeting at the donor/acceptor interface will not be ultimately bound to form a CT state, nor will this CT state instantaneously recombine. Rather, the populated CT states can either dissociate back into free carriers or recombine directly to the ground state.[15] An apparently reduced Langevin recombination is consistent with the situation in which the CT states split back into free carriers several times before a single recombination occurs. It is possible to reach an equilibrium between the free carrier densities and the population of CT states, whose density, N_{CT}, at the open-circuit voltage is given by[18]

DOI: 10.1021/acs.jpcc.5b08936
J. Phys. Chem. C 2015, 119, 26588−26597

$$N_{CT} = fN_0 \exp\left[\frac{{\sigma_{CT}}^2}{2(kT)^2}\right] \exp\left(\frac{qV_{oc} - E_{CT}}{kT}\right) \quad (7)$$

where f is the volume fraction related to the mixing ratio, N_0 is the effective density of states, and σ_{CT} is the standard deviation of the CT state energetic distribution. Based on N_{CT} given by eq 7, the recombination loss through CT states can be written as N_{CT}/τ_{CT}, where τ_{CT} is the characteristic time with which the CT state decays to the ground state and that possess typical values between 100 ps and 10 ns.[18] Note that τ_{CT} must not be confused with the overall CT lifetime, τ'_{CT}. The total rate of CT decay, $1/\tau'_{CT} = k_r + k_{sep}$, is determined by the recombination rate into the ground state, $k_r = 1/\tau_{CT}$, and by the rate of splitting back into free mobile charges, k_{sep}. Then, the open-circuit voltage V_{oc} is determined from the energy, E_{CT}, of the CT state and can be written as[18]

$$V_{oc} = E_{CT} - \frac{{\sigma_{CT}}^2}{2kT} - kT \ln\left(\frac{qfN_0L}{\tau_{CT}J_{sc}}\right) \quad (8)$$

where L is the total thickness of the OSC absorber. Remarkably, when an energetic disorder of $\sigma_{CT} > 0$ is present, the dependence of V_{oc} on temperature is no longer linear, as for the case of direct bimolecular recombination. As pointed out in ref 18, E_{CT} cannot be found simply by extrapolating the $V_{oc}(T)$ curve down to 0 K; rather, it is necessary to consider interfacial disorder when interpreting the $V_{oc}(T)$ data.

To explore the impact of CT-state-mediated recombination on the entire current−voltage characteristics, we modify eq 7 to account for any external bias. Inspired by the fact that the CT state is in equilibrium with free carriers,[18] we replace qV_{oc} with the splitting $E_{fn} - E_{fp}$ of the quasi-Fermi levels for electrons, E_{fn}, and holes, E_{fp}, at the interface at each bias voltage. As a result, the net interface recombination rates through CT states for bilayer structures can be expressed as

$$R_{CT} = \frac{fN_0}{\tau_{CT}} \exp\left[\frac{{\sigma_{CT}}^2}{2(kT)^2}\right] \exp\left(\frac{-E_{CT}}{kT}\right)\left[\exp\left(\frac{E_{fn} - E_{fp}}{kT}\right) - 1\right] \quad (9)$$

3. TEMPERATURE DEPENDENCE OF INTERFACE RECOMBINATION

As mentioned before, the determination of the temperature dependence of the open-circuit voltage is an important step in revealing the nature of interface recombination. To distinguish between the two proposed mechanisms, it is necessary to investigate which of the models is capable of reproducing the specific temperature dependence of the recombination. To that aim, experiments directly extracting the recombination rate as a function of temperature are an excellent starting point. Juška et al.[3] and Deibel et al. performed photo-charge extraction by linearly increasing voltage (photo-CELIV) experiments on polymer:[6,6]-phenyl-C_{61}-butyric acid methyl ester (polymer:PCBM) blends[3,7] sandwiched between the indium tin oxide (ITO) and aluminum (Al) contacts.[7] These experiments reveal a recombination that is substantially reduced with respect to Langevin theory. The temperature-dependent reduction factor γ, which relates the actual interface recombination rate R to the Langevin recombination rate as $R = \gamma R_L$, was found to decrease with increasing temperature.[7] This marked decrease with temperature cannot be ascribed to an encounter-limited recombination R_{int} (eq 6) occurring between uniformly distributed charges.[7] Rather, one has to assume temperature-dependent mobilities to recover at least the qualitative trend in temperature.[7]

As many other experiments are also commonly evaluated in terms of a reduced Langevin recombination, it appears to be convenient to carry out the comparison between different recombination models in terms of the model-inherent reduction factor γ. Next, we demonstrate under which conditions it is indeed possible to cast model-dependent expressions for R into apparent reduction factors.

Even though not explicitly mentioned in ref 18, the rate expression of the above-described CT model can be readily cast into a Langevin reduction factor γ. We elaborate this point as follows:

According to the Boltzmann distribution, the carrier densities satisfy the expressions $n = N_0 \exp[(E_{fn} - E_L^A)/kT]$ and $p = N_0 \exp[(E_H^D - E_{fp})/kT]$. Hence, the quasi-Fermi level terms in eq 9 can be substituted by the respective carrier densities, and eq 9 can be rewritten as

$$R_{CT} = \frac{f \exp\left[\frac{{\sigma_{CT}}^2}{2(kT)^2}\right]}{N_0\tau_{CT}} \exp\left(\frac{E_b}{kT}\right)(n^A p^D - n_0^A p_0^D) \quad (10)$$

where $E_b = E_{DA} - E_{CT}$ is the binding energy of the CT state. Comparison of eq 10 with eq 6 allows us to assign the Langevin reduction factor γ_{CT} in the framework of the CT model to the expression

$$\gamma_{CT} = \frac{f \exp\left[\frac{{\sigma_{CT}}^2}{2(kT)^2}\right]}{\beta N_0\tau_{CT}} \exp\left(\frac{E_b}{kT}\right) \quad (11)$$

Thus, it is important to stress at this point that a reduced Langevin recombination rate (eq 10) readily occurs when assuming only that a CT state is involved in interface recombination as an intermediate step and that its population is in equilibrium with the free carrier concentration at each bias voltage.

Figure 2 depicts the typical evolution of the reduction factor γ_{CT} for the CT model (open circles) as a function of temperature. To best accommodate the experimentally

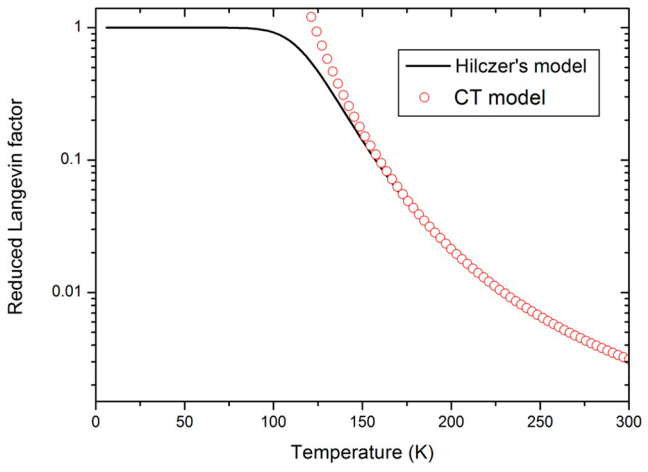

Figure 2. Temperature dependence behaviors of the Langevin reduction factor γ predicted by the continuum model[13] and the CT model.[18] Both curves are based on the parameters that fit the experimental $\gamma-T$ data of ref 7.

DOI: 10.1021/acs.jpcc.5b08936
J. Phys. Chem. C 2015, 119, 26588−26597

obtained $\gamma-T$ dependence,[7] the parameters entering eq 11 were fitted to the experimental data assuming an effective medium with a mixing ratio of $f = 1$ and a vanishing disorder of $\sigma_{CT} = 0$. The γ_{CT} factors derived from the CT model inherently reproduce the desired reduction of γ_{CT} with increasing temperature, even without implicitly invoking a temperature-activated mobility.

However, it is important to keep in mind that the CT model becomes invalid at low temperatures. When going to low temperatures, the supply of carriers meeting each charge becomes scarce because of the profoundly reduced mobilities. This prevents the achievement of equilibrium between free charges and CT states. Rather, recombination becomes limited by the first encounter,[13] that is, the Langevin reduction factor approaches unity. Consequently, the gradient concentration model[7] relying on encounter-limited recombination reflects the low-temperature limit of γ correctly.

We illustrate the transition from a recombination mediated by an intermediate CT state to a recombination being diffusion-limited by means of the analytical continuum approach of Hilczer and Tachiya.[13] The underlying model is an extension of the Onsager model that explicitly considers the rates of formation, dissociation, and recombination of an intermediate state, and is, hence, expected to capture the general trend of recombination with temperature. Note that the CT model assigns this intermediate state to the interfacial CT state; consequently, the separation of the bound electrons and holes is inherently associated with the extension of the CT-state wave function. Hilczer and Tachiya[13] provided a general estimation for the binding energy E_b' of the intermediate state as a function of the separation of electron and hole in the bound state and the electric field. From that, they derived a recombination reduction factor γ_{HT} as[13]

$$\gamma_{HT} = \frac{1}{1 - \exp\left(\frac{-E_b'}{kT}\right) + \frac{\beta}{4\pi R^3 k_r}\exp\left(\frac{-E_b'}{kT}\right)} \tag{12}$$

where k_r describes the rate at which the bound electron–hole pair recombines into the ground state and $E_b' = q^2/4\pi\varepsilon R$ is defined as the binding energy of the electron–hole pair, with R being the separation of the electron and hole. Equation 12 significantly refines the most commonly used formulations[30,31] for organic solar cells that rely on the original models of Onsager[6] and Braun.[32] The temperature dependence of γ_{HT} as defined in eq 12 is plotted in Figure 2 (black line). As was done for the γ_{CT} case before, the values of the parameters entering γ_{HT}, namely, E_b' and $\beta(k_r R)^{-1}$, were chosen to best reproduce the experimental reference data.[13]

For low temperatures, γ_{HT} approaches unity, as expected for the diffusion-limited regime. However, at temperatures exceeding ca. 150 K, γ_{HT} exhibits a rapid decay with temperature that essentially coincides with the behavior of γ_{CT} versus T. In fact, it can be shown that γ_{HT} can be cast into the same functional form as γ_{CT} in the considered temperature range (see Supporting Information). Then, the expressions for both γ_{CT} and γ_{HT} are consistent in that the exponential term containing the binding energy of the intermediate state, be that the CT state or the energy of the bound electron–hole pair, contributes to the temperature dependence of γ. However, the CT model contains a second T-dependent contribution given by the exponential factor $\exp\{(\sigma_{CT}^2)/[2(kT)^2]\}$ related to the energy disorder σ_{CT}. This factor contributes to a decrease in γ with increasing T, because elevated temperatures lead to an increasing population of CT states with lower binding energies.

Having established the qualitative trends, we now turn to a discussion of the quantitative values provided by the CT model. Fitting the experimentally obtained reduction factors[7] with eq 11 assuming temperature-independent mobilities, a mixing ratio of $f = 1$ in the blend, and a sharply defined CT-state energy ($\sigma_{CT} = 0$) gives a reasonable CT-state binding energy of $E_b \approx 0.12$ eV. However, based on the β value given in ref 7, the fitted value of $\tau_{CT} \approx 400$ ns at room temperature is larger than expected. One possible reason could lie in the simplifications that we made prior to parameter fitting against the experiment. In realistic BHJ devices, neither the temperature dependence of the charge mobilities nor the energetic disorder σ_{CT} and blend morphology can readily be omitted.

4. DRIFT-DIFFUSION MODELING

Despite the compelling evidence that CT states and their dynamics determine recombination, the disentanglement of possible contributions indirectly affecting interface recombination in BHJs remains difficult. It thus appears to be useful to turn to organic bilayer solar cells, for which bulk morphology, spatial disorder, and inhomogeneities in charge-carrier density and mobility are expected to play a subordinate role. In this section, we verify the applicability of the CT recombination model by incorporating it into drift-diffusion modeling and employ our modeling investigation to a simple bilayer OSC, in which the planar donor/acceptor interface is located at only one position. To focus our modeling investigations on the effects of interface recombination, we also simplify the consideration of other physical factors. For example, the mobility is assumed to be constant and independent of the temperature and the electrical field. Neither injection/extraction barriers at contacts nor SRH recombination occur in the device.

The bilayer system analyzed in this article is based on the system of pentacene and fullerene C_{60}. The material parameters used in the simulations are listed in Table 1.

Table 1. Modeling Parameters of a Bilayer OSC with a Structure of Glass/ITO (150 nm)/Pentacene (50 nm)/C_{60} (50 nm)/BCP (10 nm)/Al[33,34] [a]

	donor (pentacene)	acceptor (C_{60})
relative permittivity	3.5	4.4
electron affinity (eV)	3.3	4.3
band gap (eV)	1.9	1.7
effective density of states, N_0 (cm^{-3})	10^{21}	10^{21}
electron mobility ($cm^2\ V^{-1}\ s^{-1}$)	10^{-4}	10^{-4}
hole mobility ($cm^2\ V^{-1}\ s^{-1}$)	10^{-1}	10^{-4}
doping (cm^{-3})	intrinsic	intrinsic
exciton diffusion length (nm)	65	40
	top contact	bottom contact
work function (eV)	5.4	4.2
electron recombination velocity (cm/s)	10^7 (ohmic)	10^7 (ohmic)
hole recombination velocity (cm/s)	10^7 (ohmic)	10^7 (ohmic)
	CT state at the interface	
binding energy, E_b (eV)	0.15	
energetic disorder, σ_{CT} (eV)	0.05	

[a] ITO and BCP/Al at both contacts are treated as ohmic contacts, and their optical constants were used in the optical model to obtain the generation rates within the pentacene/C_{60} layers.

DOI: 10.1021/acs.jpcc.5b08936
J. Phys. Chem. C 2015, 119, 26588–26597

4.1. Numerical Implementation. The numerical simulation in this work is based on a two-dimensional (2D) drift-diffusion model that solves three fundamental semiconductor equations (Poisson equation and current continuity equations for electrons and holes) and one additional exciton diffusion equation. These 2D partial differential equations are discretized by the finite-difference method using a five-point scheme[35] and an improved iterative algorithm that combines the advantages of Newton's method and Gummel's method.[36] At each iteration, the variables used for the next iteration are solved by the strongly implicit method, which presents a relatively high convergence speed.[37]

The recombination in the bulk of OSCs is still described by the Langevin model according to eq 2. The interface recombination, as described in either eq 6 without specifying the origin of γ or eq 9 assuming the involvement of the CT state, requires electrons from the acceptor side and holes from the donor side. In the special case of the bilayer solar cell, eq 9 is employed only at the donor/acceptor interface with a mixing fraction of $f = 1$. The associated density of the interface recombination current J_{intR} is given for the CT model by

$$J_{intR} = qR_{CT}\Delta d \tag{13}$$

where Δd is the distance between two adjacent donor/acceptor molecules at the interface. In our simulation, this molecular distance Δd was estimated to be 1 nm. J_{intR} must be incorporated such that current continuity across the interface is guaranteed.

In terms of boundary conditions, the general surface recombination model is used at the contacts.[38] Throughout this work, we assume ohmic contacts that correspond to surface recombination velocities of 10^7 cm/s for each carrier (Table 1). Zero exciton flow is taken as the boundary condition for the exciton diffusion equation. To obtain the photon distribution within the device, we employ the transfer matrix method, which considers internal reflections and transmissions between each layer.[39] The optical constants for each layer are based on reported values.[34,40−42]

4.2. Results and Discussion. *4.2.1. Current−Voltage Characteristics.* The drift-diffusion model provides a way to assess the implications of local, CT-state-based interface recombination for the macroscopic performance of the entire device, in particular for the current−voltage (J−V) characteristics. In this section, the effects of the interface recombination due to the CT model are analyzed and compared to the "plain" reduced Langevin recombination model given by eq 6.

Figure 3 shows how the J−V characteristics evolve with varying Langevin reduction factor γ (solid lines) and for CT-state-mediated interface recombination according to eq 9 with different τ_{CT} values (dashed lines). It is readily evident that, in both cases, the J−V curves change considerably within the given parameter range. Considering typical V_{oc} values for the bilayer pentacene/C_{60} OSC (~0.37 V),[43] we identified corresponding γ values of around 10^{-2} or τ_{CT} values between 1 and 10 ns from the set of curves displayed in Figure 3 (dashed box). The J−V curves associated with these γ and τ_{CT} values excellently match the experimentally determined characteristics[43] in the power quadrant in terms of J_{sc} and V_{oc} alone. (The fill factor was somewhat overestimated for the ideal assumption of ohmic contacts.) Moreover, the determined γ and τ_{CT} values are in good agreement within their reported ranges mentioned in section 2.2 and are also consistent when

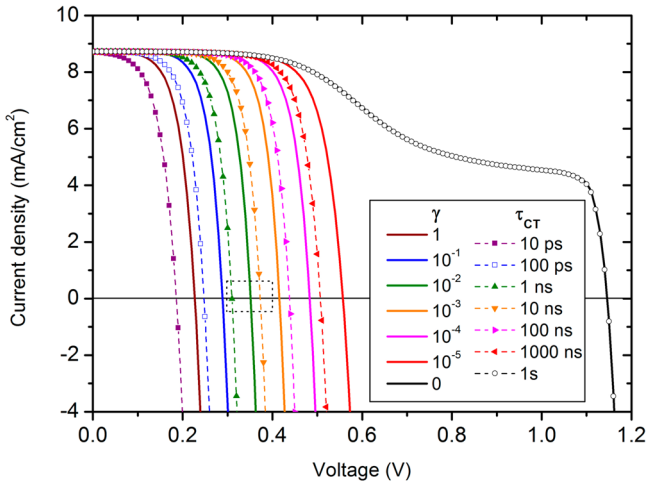

Figure 3. J−V curves simulated by a plain reduced Langevin recombination model for different values of γ (solid lines) and by the CT model with different values of τ_{CT} (dashed lines with symbols). Interface recombination is absent for $\gamma = 0$ and almost zero for $\tau_{CT} = 1$ s. The dotted box shows the range of experimental V_{oc} values reported for the bilayer pentacene/C_{60} OSC.[43]

related to each other using eq 11. The V_{oc} values obtained from the simulation match exactly the values predicted with eq 8.

As seen from Figure 3, the open-circuit voltages and, thus, device efficiencies increase when reducing the interfacial recombination rates. According to the empirical expression for the fill factor,[44] FF is expected to show the same trend as V_{oc} as long as the series resistance and the shunt resistance do not vary significantly. This is indeed the case here, except in the situations in which interface recombination is entirely absent ($\gamma = 0$ and $\tau_{CT} = 1$ s in Figure 3); then, the FF drops abruptly and an S-shaped J−V curve appears (Figure 3).

We attribute the occurrence of the S-shape to the large band offsets at the interface. According to the parameters in Table 1, these offsets amount to 1.0 eV between LUMO levels of pentacene and C_{60} and to 0.8 eV between the HOMO levels. To illustrate the origin of the S-shape, we plot in Figure 4a,b the spatial dependence of the transport levels, the quasi- Fermi levels (a), and the carrier concentration perpendicular to the electrodes (b) for a large forward bias voltage of 0.8 V, i.e., a bias near the built-in voltage. With the donor layer depicted in the left half and the acceptor in the right half, the photogenerated holes travel from the donor/acceptor interface located at the center at 50 nm to the left, while electrons move from the center to the right; accordingly, the photo current is oriented from the right to the left (Figure 4a). At biases near or exceeding the built-in voltage, the photogenerated charges exit the device essentially due to diffusion (process I in Figure 4c) as the electric field is either very small or oriented such that its counteracts the motion of photogenerated carriers to the collecting contacts. If interface recombination is absent, there is essentially one interface-related current contribution that counteracts the photocurrent, schematically illustrated as process **II** in the right panels of Figure 4c. Mobile charges located at the interface can surmount the barrier associated with the LUMO and HOMO offsets, be that due to diffusion or a thermally activated hopping process. Consequently, such charges travel in a direction opposite to the desired one. If, as indicated earlier, the offsets ΔLUMO and ΔHOMO between the transport levels are rather large, i.e., in the order

DOI: 10.1021/acs.jpcc.5b08936
J. Phys. Chem. C 2015, 119, 26588−26597

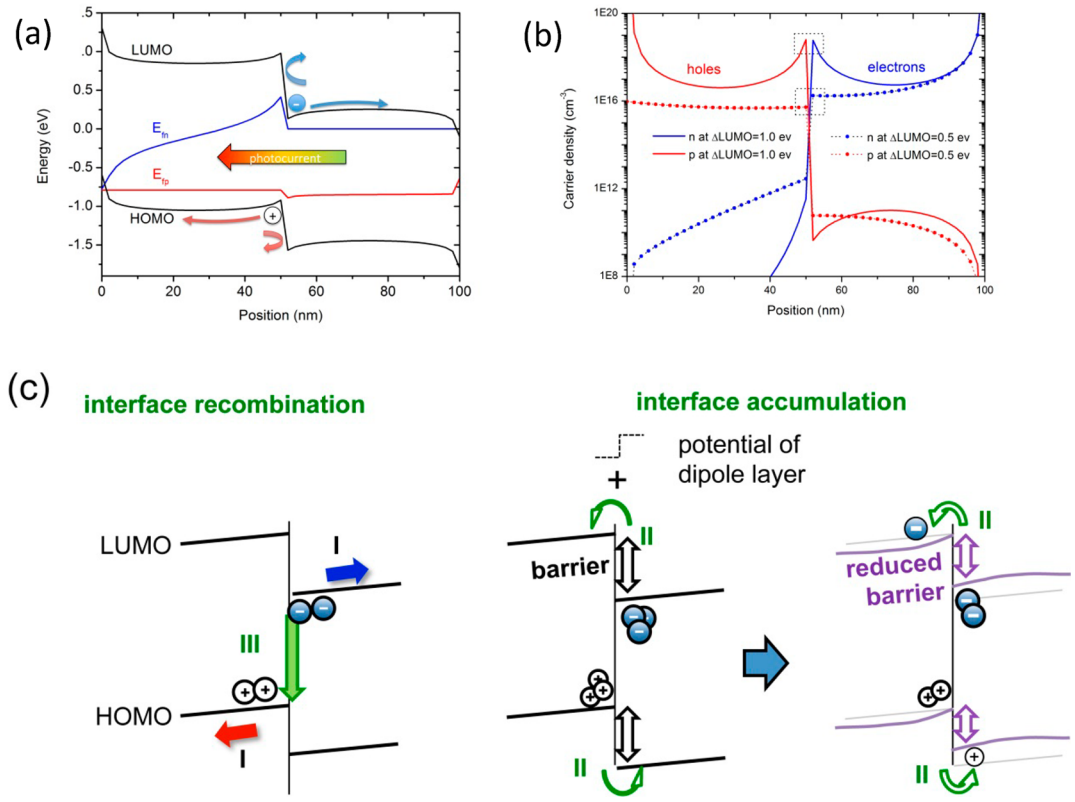

Figure 4. (a) Energy band diagram and positions of the quasi-Fermi levels in the bilayer OSC at 0.8 V under illumination in the absence of interface recombination. (b) Carrier profiles at 0.8 V under illumination without considering interface recombination. Shown are the carrier concentrations for a large LUMO offset, ΔLUMO = 1.0 eV (solid lines), and a considerably smaller LUMO offset, ΔLUMO = 0.5 eV (dotted lines). The dotted boxes highlight the corresponding charge densities at the interface that give rise to a dipole layer. (c) Schematic illustration of loss processes at the donor/acceptor interface for external biases close to or larger than the built-in voltage. The left panel depicts the situation with interface recombination, whereas the right panels show the situation without interface recombination and substantial band offsets.

of the build-in voltage $\approx q^{-1}E_{DA}$, the likelihood of overcoming the barriers is very small.

This causes a strong accumulation of carriers of opposing polarity at each side of the interface, as can be seen from the carrier concentrations (solid lines) in the boxed region in Figure 4b, and gives rise to a dipole layer associated with a large dipole density. Such accumulated interface charges cause a rapid change in the electrostatic potential at the interface. In the limiting case of a point-dipole layer, one would observe an abrupt step-like potential jump (indicated as dashed line in center panel of Figure 4c). Due to the superimposed dipole-layer potential, the modified energy of transport levels at the interface, shown as purple line in right panel of Figure 4c, gives rise to an effectively reduced level offset.[45] The numerical simulation also verifies this by revealing that ΔLUMO in Figure 4a is reduced by ∼0.16 eV. The correspondingly enhanced loss process **II** gives rise to a reduced net current and, thus, to a lower FF.[46]

When we keep neglecting interface recombination and artificially reduce the band offsets to values smaller than 0.5 eV (by increasing the electron affinity of the donor), carriers can surmount the barriers at the interface much more easily (dotted lines in Figure 4b) and, in doing so, prevent a marked accumulation at the interface; Figure 4b indicates that the charge density drops by 3 orders of magnitude in the dotted region (cf. dotted and solid lines). Thus, the current contribution due to loss process **II** will not be boosted in this bias region and the $J-V$ curve will retain a diode-like shape.

Alternatively, also the incorporation of interface recombination, indicated as process **III** in the left panel of Figure 4c, prevents a profound accumulation of charges at the interface, in particular for large forward biases. Thus, process **II** will not be accumulation-activated and the $J-V$ curve will keep a large FF.

4.2.2. Temperature-Dependent V_{oc}. Having established the shape of the $J-V$ curve for relevant CT life times, we are also able to extract the temperature dependence of the open-circuit voltage due to interface recombination through CT states directly from drift-diffusion simulations. Figure 5 compares the resulting evolution of V_{oc} as a function temperature to other interface recombination scenarios.

As indicated in section 2, inspection of the experimentally obtained $V_{oc}-T$ relations yields important clues to the nature of interface recombination. In essence, the identification of the relevant interface recombination mechanism is guided by two questions: First, one has to discriminate between linear and nonlinear behaviors. In a second step, the value of the extrapolated activation energy hints at the characteristic energy in the system and, thus, the dominant processes involved in recombination.

For example, the absence of interface recombination yields a linear relation (open circles in Figure 5). The activation energy, E_a, corresponds exactly to $E_g(C_{60})$, that is, the band gap determining bulk recombination. Once interface recombination is present, it is found to dominate the current near open-circuit conditions. Thus, the open-circuit voltages extracted from the simulated $J-V$ curves agree with the values due to one-step

DOI: 10.1021/acs.jpcc.5b08936
J. Phys. Chem. C 2015, 119, 26588−26597

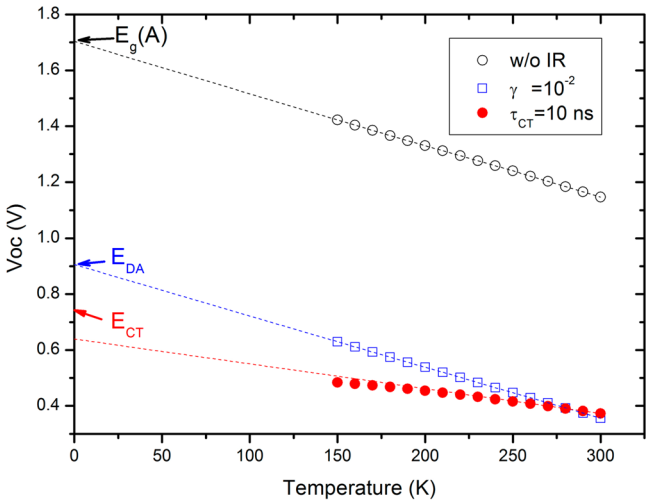

Figure 5. Temperature dependence behaviors of V_{oc} obtained from three different models relying on the parameters for the pentacene/C_{60} solar cell (cf. Table 1): no interface recombination (open circles), reduced Langevin recombination assuming a single-step bimolecular interface recombination with γ = 0.01 (squares), and CT-state-mediated recombination with τ_{CT} = 10 ns and σ_{CT} = 50 mV (solid circles). E_g(A) denotes the acceptor band gap, which is smaller than the donor band gap. E_{DA} is the donor/acceptor effective band gap.

bimolecular recombination (eq 1) and the CT model (eq 8), respectively. To date, the indicators associated with each of the interface recombination scenarios have been experimentally observed.

In the case of the one-step bimolecular recombination, we expect linear V_{oc}-T relation according to the theoretical discussion in section 2. Extrapolation leads to an activation energy E_a that corresponds to the effective band gap E_{DA} (squares in Figure 5). Indeed, such a behavior has been reported for bulk heterojunction solar cells made of a multitude of different small molecule donor/acceptor pairs.[12] For each of these devices, a linear $V_{oc}-T$ relation was obtained within the measured temperature range. The extrapolated activation energy agreed, within error bars, with the value of E_{DA} obtained from the difference in the measured acceptor electron affinity and donor ionization potential.[12]

The CT model, on the other hand, gives rise to a small deviation from the linear $V_{oc}(T)$ relation. Nor does the extrapolation of the curve to 0 K yield E_{CT} (compare position of arrow and solid circles in Figure 5). Only for a vanishing energetic disorder, σ_{CT} = 0 meV, does $E_a = E_{CT}$; otherwise, the much more likely case of energetic disorder of the CT state[18] (σ_{CT} = 50 meV was used in this simulation) causes a sublinear decrease of V_{oc} with increasing temperature. Such nonlinear behavior has been observed in polymer donor:PCBM blends,[16] for which the measured, apparently temperature-dependent E_{CT} is actually given by $E_{CT} - \sigma^2/2kT$.[18]

It is difficult to find an overall rationale for the apparently opposing outcomes of the two experiments in refs 12 and 16, in particular, because there is no hint whether a certain type of recombination prevails for a specific material combination. This inspired us to closely inspect the $V_{OC}-T$ measurements put forward in refs 12 and 16 once more. Considering the fingerprint of recombination mechanisms collected above, it appears to be crucial to carefully identify the temperature range in which (i) a nonlinear behavior can be safely distinguished from a linear one and (ii) both recombination models are valid.

We illustrate this assessment in Figure 5. Inspecting V_{oc} determined for T > 150 K within the CT model, we clearly identify the nonlinear decrease. However, when considering the smaller temperature interval of 200 < T < 300 K, the relation is apparently linear and would support picking the wrong mechanism. On the other hand, the CT model fails when going to too low temperatures, i.e., in our case below 150 K (cf. Figure 2). Then, the extrapolation incorporating values from such a low temperature leads to an erroneous activation energy.

4.2.3. Impact of the Mixing Ratio at the Donor/Acceptor Interface. In the previous section, we discussed a bilayer OSC with a perfectly ordered donor/acceptor interface containing a volume fraction of f_{int} = 1. The CT recombination model allows one to probe the impact of different degrees of donor/acceptor mixing at the interface on the performance of a bilayer solar cell. In the spirit of Haerter et al.,[47] the degree of donor/acceptor mixing is tuned by varying the volume fraction f_{int} in the range of 0−1.

Reducing the active interface directly affects the interface recombination rate (eq 10) and the rate of exciton dissociation through CT states, as both quantities are proportional to f_{int}. Figure 6a depicts the evolution of the $J-V$ characteristics with decreasing f_{int}. Reducing the value of f_{int} from 1 by 3 orders of magnitude gives rise to an increase in V_{oc} due to an increasingly suppressed interface recombination (see Figure 6b). At the

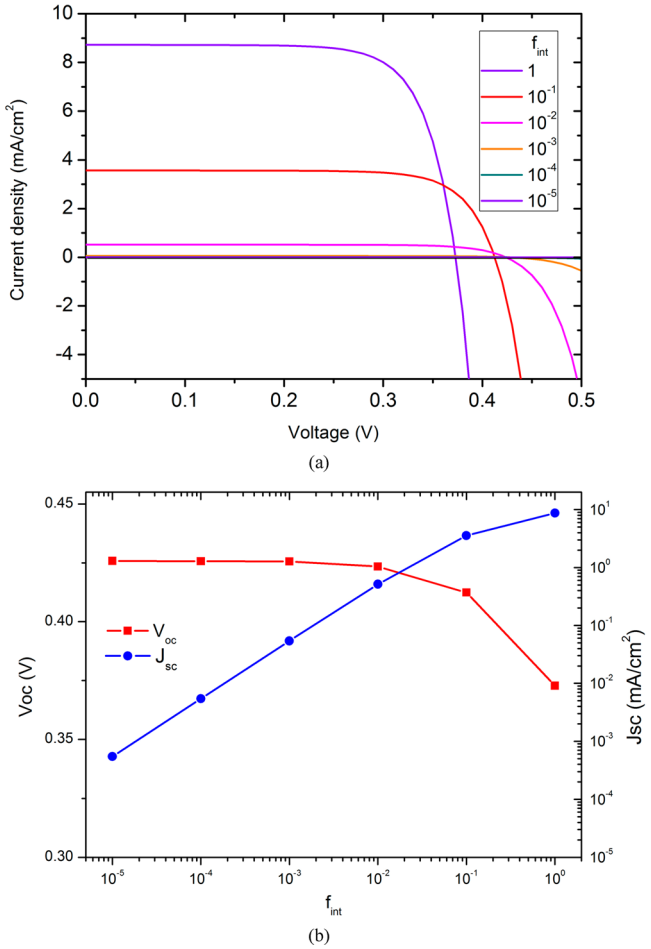

Figure 6. (a) $J-V$ curves for different degrees (f_{int}) of donor/acceptor mixing at the interface of the bilayer solar cell shown in Figure 4. (b) V_{oc} and J_{sc} modeled with different values of f_{int}.

DOI: 10.1021/acs.jpcc.5b08936
J. Phys. Chem. C 2015, 119, 26588−26597

same time, the short-circuit current J_{sc} decreases as the exciton dissociation through CT states is reduced. Remarkably, when f_{int} is reduced even further (i.e., $f_{int} < 10^{-3}$), J_{sc} becomes strictly proportional to f_{int}. That is, sites that are able to dissociate excitons become so scarce that only the fraction of excitons corresponding to f_{int} is split. In accord with eq 8, this gives rise to an almost constant value of V_{oc} (Figure 6b).

5. CONCLUSIONS

In this work, we explore the impact of the recombination model suggested recently by Burke et al.,[18] in which interface recombination is a two-step process involving a charge-transfer state, on the $J-V$ characteristics of organic solar cells. Toward that aim, we extended the model such that it can be employed also when operating the solar cell at external biases other than V_{oc}. We demonstrate that the involvement of the intermediate CT states is a plausible origin of the apparently reduced Langevin recombination. The characteristic temperature dependence of the corresponding Langevin reduction factor γ is predominantly determined by the binding energy of the electron and the hole bound in the CT state and the spread of the CT-state energies due to disorder. Even when temperature-independent mobilities are assumed, the reduction of γ with increasing temperature can be qualitatively reproduced. For a quantitative prediction, however, additional knowledge about (at least) the actual temperature dependence and the degree of disorder in the CT-state energies is required. Moreover, for $T >$ 150 K, the predicted evolution of $\gamma-T$ coincides with the continuum model of Hilczer and Tachiya.[13]

Once incorporated in device simulations, the model allows realistic $J-V$ curves of bilayer OSCs to be quantitatively reproduced. It further demonstrates that the CT recombination model leads to qualitatively similar $J-V$ curves as the reduced Langevin recombination model relying on encounter-limited bimolecular recombination. In both models, the interface recombination is shown not only to determine V_{OC}, but also to affect the fill factor.

Future work will include the experimental determination of interface recombination in bilayer OSCs to further develop the theory presented in this article. Furthermore, the 2D drift-diffusion model presented here will be adapted to enaing of ble the model BHJ devices by taking bulk morphology effects into account.

■ ASSOCIATED CONTENT

Supporting Information

Derivation of an approximate Langevin reduction factor for the continuum model of Hilczer and Tachiya[13] The Supporting Information is available free of charge on the ACS Publications website at DOI: 10.1021/acs.jpcc.5b08936.

Derivation of the Langevin reduction factor from Hilczer and Tachiya's continuum method (PDF)

■ AUTHOR INFORMATION

Corresponding Authors

*E-mail: karin.zojer@tugraz.at (K.Z.).
*E-mail: madsen@mci.sdu.dk (M.M.).

Notes

The authors declare no competing financial interest.

■ ACKNOWLEDGMENTS

The work was supported by the SDU2020 project "Production of Next-Generation Energy Devices" and the Austrian Science Fund through Elise Richter Fellowship V317-N20. The authors acknowledge Iris Hehn for her contributions to the drift-diffusion model of OSCs. This project has received funding from the European Union Seventh Framework Programme under grant agreement no. 607232.

■ REFERENCES

(1) Bartelt, J. A.; Lam, D.; Burke, T. M.; Sweetnam, S. M.; McGehee, M. D. Charge-Carrier Mobility Requirements for Bulk Heterojunction Solar Cells with High Fill Factor and External Quantum Efficiency > 90%. *Adv. Energy Mater.* **2015**, *5*, 1500577-1−1500577-10.

(2) Vandewal, K.; Tvingstedt, K.; Gadisa, A.; Inganäs, O.; Manca, J. V. On the Origin of the Open-Circuit Voltage of Polymer−Fullerene Solar Cells. *Nat. Mater.* **2009**, *8*, 904−909.

(3) Juška, G.; Arlauskas, K.; Stuchlik, J.; Österbacka, R. Non-Langevin Bimolecular Recombination in Low-Mobility Materials. *J. Non-Cryst. Solids* **2006**, *352*, 1167−1171.

(4) Murthy, D. H. K.; Melianas, A.; Tang, Z.; Juška, G.; Arlauskas, K.; Zhang, F.; Siebbeles, L. D. a; Inganäs, O.; Savenije, T. J. Origin of Reduced Bimolecular Recombination in Blends of Conjugated Polymers and Fullerenes. *Adv. Funct. Mater.* **2013**, *23*, 4262−4268.

(5) Lakhwani, G.; Rao, A.; Friend, R. H. Bimolecular Recombination in Organic Photovoltaics. *Annu. Rev. Phys. Chem.* **2014**, *65*, 557−581.

(6) Onsager, L. Deviations from Ohm's Law in Weak Electrolytes. *J. Chem. Phys.* **1934**, *2*, 599−615.

(7) Deibel, C.; Wagenpfahl, A.; Dyakonov, V. Origin of Reduced Polaron Recombination in Organic Semiconductor Devices. *Phys. Rev. B: Condens. Matter Mater. Phys.* **2009**, *80*, 075203-1−075203-7.

(8) Heiber, M. C.; Baumbach, C.; Dyakonov, V.; Deibel, C. Encounter-Limited Charge-Carrier Recombination in Phase-Separated Organic Semiconductor Blends. *Phys. Rev. Lett.* **2015**, *114*, 136602-1−136602-5.

(9) Juška, G.; Genevičius, K.; Nekrašas, N.; Sliaužys, G.; Österbacka, R. Two Dimensional Langevin Recombination in Regioregular Poly(3-hexylthiophene). *Appl. Phys. Lett.* **2009**, *95*, 013303-1−013303-3.

(10) Nyman, M.; Sandberg, O. J.; Österbacka, R. 2D and Trap-Assisted 2D Langevin Recombination in Polymer:Fullerene Blends. *Adv. Energy Mater.* **2015**, *5*, 1400890-1−1400890-7.

(11) Scharber, M. C.; Mühlbacher, D.; Koppe, M.; Denk, P.; Waldauf, C.; Heeger, A. J.; Brabec, C. J. Design Rules for Donors in Bulk-Heterojunction Solar Cells—Towards 10% Energy-Conversion Efficiency. *Adv. Mater.* **2006**, *18*, 789−794.

(12) Widmer, J.; Tietze, M.; Leo, K.; Riede, M. Open-Circuit Voltage and Effective Gap of Organic Solar Cells. *Adv. Funct. Mater.* **2013**, *23*, 5814−5821.

(13) Hilczer, M.; Tachiya, M. Unified Theory of Geminate and Bulk Electron−Hole Recombination in Organic Solar Cells. *J. Phys. Chem. C* **2010**, *114*, 6808−6813.

(14) Clarke, T. M.; Durrant, J. R. Charge Photogeneration in Organic Solar Cells. *Chem. Rev.* **2010**, *110*, 6736−6767.

(15) Deibel, C.; Strobel, T.; Dyakonov, V. Role of the Charge Transfer State in Organic Donor−Acceptor Solar Cells. *Adv. Mater.* **2010**, *22*, 4097−4111.

(16) Vandewal, K.; Tvingstedt, K.; Gadisa, A.; Inganäs, O.; Manca, J. V. Relating the Open-Circuit Voltage to Interface Molecular Properties of Donor:Acceptor Bulk Heterojunction Solar Cells. *Phys. Rev. B: Condens. Matter Mater. Phys.* **2010**, *81*, 125204-1−125204-8.

(17) Vandewal, K.; Widmer, J.; Heumueller, T.; Brabec, C. J.; McGehee, M. D.; Leo, K.; Riede, M.; Salleo, A. Increased Open-Circuit Voltage of Organic Solar Cells by Reduced Donor−Acceptor Interface Area. *Adv. Mater.* **2014**, *26*, 3839−3843.

(18) Burke, T. M.; Sweetnam, S.; Vandewal, K.; McGehee, M. D. Beyond Langevin Recombination: How Equilibrium Between Free Carriers and Charge Transfer States Determines the Open-Circuit

DOI: 10.1021/acs.jpcc.5b08936
J. Phys. Chem. C 2015, 119, 26588−26597

Voltage of Organic Solar Cells. *Adv. Energy Mater.* **2015**, *5*, 1500123-1−1500123-12.
(19) Pauwels, H.; Vanhoutte, G. The Influence of Interface States and Energy Barriers on the Efficiency of Heterojunction Solar Cells. *J. Phys. D: Appl. Phys.* **1978**, *11*, 649−667.
(20) Rau, U.; Jasenek, A.; Schock, H.; Engelhardt, F.; Meyer, T. Electronic Loss Mechanisms in Chalcopyrite Based Heterojunction Solar Cells. *Thin Solid Films* **2000**, *361-362*, 298−302.
(21) Scheer, R. Activation Energy of Heterojunction Diode Currents in the Limit of Interface Recombination. *J. Appl. Phys.* **2009**, *105*, 104505-1−104505-6.
(22) Wilhelm, H.; Schock, H.-W.; Scheer, R. Interface Recombination in Heterojunction Solar Cells: Influence of Buffer Layer Thickness. *J. Appl. Phys.* **2011**, *109*, 084514-1−084514-6.
(23) Fonash, S. *Solar Cell Device Physics*, 2nd ed.; Elsevier, New York, 2010.
(24) Burgelman, M.; Nollet, P.; Degrave, S. Modelling Polycrystalline Semiconductor Solar Cells. *Thin Solid Films* **2000**, *361−362*, 527−532.
(25) Scheer, R. Towards an Electronic Model for CuIn1−xGaxSe2 Solar Cells. *Thin Solid Films* **2011**, *519*, 7472−7475.
(26) Gunawan, O.; Todorov, T. K.; Mitzi, D. B. Loss Mechanisms in Hydrazine-Processed $Cu_2ZnSn(Se,S)_4$ Solar Cells. *Appl. Phys. Lett.* **2010**, *97*, 233506-1−233506-3.
(27) Deibel, C.; Dyakonov, V. Polymer−Fullerene Bulk Heterojunction Solar Cells. *Rep. Prog. Phys.* **2010**, *73*, 096401-1−096401-39.
(28) Staudigel, J.; Stößel, M.; Steuber, F.; Simmerer, J. A Quantitative Numerical Model of Multilayer Vapor-Deposited Organic Light Emitting Diodes. *J. Appl. Phys.* **1999**, *86*, 3895−3910.
(29) Tress, W.; Leo, K.; Riede, M. Optimum Mobility, Contact Properties, and Open-Circuit Voltage of Organic Solar Cells: A Drift-Diffusion Simulation Study. *Phys. Rev. B: Condens. Matter Mater. Phys.* **2012**, *85*, 155201-1−155201-11.
(30) Barker, J.; Ramsdale, C. M.; Greenham, N. C. Modeling the Current−Voltage Characteristics of Bilayer Polymer Photovoltaic Devices. *Phys. Rev. B: Condens. Matter Mater. Phys.* **2003**, *67*, 075205-1−075205-9.
(31) Koster, L. J. A.; Smits, E. C. P.; Mihailetchi, V. D.; Blom, P. W. M. Device Model for the Operation of Polymer/Fullerene Bulk Heterojunction Solar Cells. *Phys. Rev. B: Condens. Matter Mater. Phys.* **2005**, *72*, 085205-1−085205-9.
(32) Braun, C. L. Electric Field Assisted Dissociation of Charge Transfer States as a Mechanism of Photocarrier Production. *J. Chem. Phys.* **1984**, *80*, 4157−4161.
(33) Kawata, S.; Pu, Y.-J.; Ohashi, C.; Nakayama, K.; Hong, Z.; Kido, J. A Morphology Control Layer of a Pyrene Dimer Enhances the Efficiency in Small Molecule Organic Photovoltaic Cells. *J. Mater. Chem. C* **2014**, *2*, 501−509.
(34) Huang, J.; Yu, J.; Guan, Z.; Jiang, Y. Improvement in Open Circuit Voltage of Organic Solar Cells by Inserting a Thin Phosphorescent Iridium Complex Layer. *Appl. Phys. Lett.* **2010**, *97*, 143301-1−143301-3.
(35) Selberherr, S. *Analysis and Simulation of Semiconductor Devices*; Springer-Verlag, Wien, Austria, 1984.
(36) Liu, Y.; Sun, Y.; Rockett, A. An Improved Algorithm for Solving Equations for Intra-Band Tunneling Current in Heterojunction Solar Cells. *Thin Solid Films* **2012**, *520*, 4947−4950.
(37) Stone, H. L. Iterative Solution of Implicit Approximations of Multidimensional Partial Differential Equations. *SIAM J. Numer. Anal.* **1968**, *5*, 530−558.
(38) Wagenpfahl, A.; Rauh, D.; Binder, M.; Deibel, C.; Dyakonov, V. S-Shaped Current-Voltage Characteristics of Organic Solar Devices. *Phys. Rev. B: Condens. Matter Mater. Phys.* **2010**, *82*, 115306-1−115306-8.
(39) Pettersson, L. A. A.; Roman, L. S.; Inganäs, O.; Introduction, I.; Inganäs, O. Modeling Photocurrent Action Spectra of Photovoltaic Devices Based on Organic Thin Films. *J. Appl. Phys.* **1999**, *86*, 487−496.
(40) Ren, S. L.; Wang, Y.; Rao, a. M.; McRae, E.; Holden, J. M.; Hager, T.; Wang, K.; Lee, W. T.; Ni, H. F.; Selegue, J.; et al. Ellipsometric Determination of the Optical Constants of C_{60} (Buckminsterfullerene) Films. *Appl. Phys. Lett.* **1991**, *59*, 2678−2680.
(41) Faltermeier, D.; Gompf, B.; Dressel, M.; Tripathi, A. K.; Pflaum, J. Optical Properties of Pentacene Thin Films and Single Crystals. *Phys. Rev. B: Condens. Matter Mater. Phys.* **2006**, *74*, 125416-1−125416-6.
(42) Datta, D.; Iyer, S. S. K.; Kumar, S. Role of Exciton Blocking Layers as Optical Spacer in CuPc/C_{60} Based Organic Solar Cells. In *2010 35th IEEE Photovoltaic Specialists Conference*; IEEE Press: Piscataway, NJ, 2010; pp 000508−000512.
(43) Yoo, S.; Domercq, B.; Kippelen, B. Efficient Thin-Film Organic Solar Cells Based on Pentacene/C_{60} Heterojunctions. *Appl. Phys. Lett.* **2004**, *85*, 5427-1−5427-3.
(44) Green, M. A. Accuracy of Analytical Expressions for Solar Cell Fill Factors. *Sol. Cells* **1982**, *7*, 337−340.
(45) Hehn, I. Investigation of the Impact of Interface Dipole Layers on the Performance of Organic Solar Cells by Drift-Diffusion Simulations, Master's Thesis, Graz University of Technology, Graz, Austria, 2012.
(46) Kumar, A.; Sista, S.; Yang, Y. Dipole Induced Anomalous S-Shape *I*−*V* Curves in Polymer Solar Cells. *J. Appl. Phys.* **2009**, *105*, 094512-1−094512-6.
(47) Haerter, J. O.; Chasteen, S. V.; Carter, S. a.; Scott, J. C. Numerical Simulations of Layered and Blended Organic Photovoltaic Cells. *Appl. Phys. Lett.* **2005**, *86*, 164101-1−164101-3.

DOI: 10.1021/acs.jpcc.5b08936
J. Phys. Chem. C 2015, 119, 26588−26597